



Future increases in Arctic lightning and fire risk for permafrost carbon

Yang Chen¹✉, David M. Romps^{2,3}, Jacob T. Seeley^{2,5}, Sander Veraverbeke⁴, William J. Riley³, Zelalem A. Mekonnen³ and James T. Randerson¹

Lightning is an indicator and a driver of climate change. Here, using satellite observations of lightning flash rate and ERA5 reanalysis, we find that the spatial pattern of summer lightning over northern circumpolar regions exhibits a strong positive relationship with the product of convective available potential energy (CAPE) and precipitation. Applying this relationship to Climate Model Intercomparison Project Phase 5 climate projections for a high-emissions scenario (RCP8.5) shows an increase in CAPE ($86 \pm 22\%$) and precipitation ($17 \pm 2\%$) in areas underlain by permafrost, causing summer lightning to increase by $112 \pm 38\%$ by the end of the century (2081–2100). Future flash rates at the northern treeline are comparable to current levels 480 km to the south in boreal forests. We hypothesize that lightning increases may induce a fire–vegetation feedback whereby more burning in Arctic tundra expedites the northward migration of boreal trees, with the potential to accelerate the positive feedback associated with permafrost soil carbon release.

Permafrost soils contain a large reservoir of organic carbon that is comparable to the total carbon content in the global atmosphere^{1–3} and considerably higher than the carbon stored in aboveground biomass in boreal forests and other high-northern-latitude terrestrial ecosystems⁴. Much of the permafrost carbon resides in Arctic tundra ecosystems across Eurasia and North America and in sparsely forested taiga ecosystems and peatlands farther south⁵. Multiple lines of observational evidence indicate that microbial decomposition of soil organic matter in permafrost-dominated ecosystems has a high sensitivity to thaw and increases in soil temperature^{6–9}. In Earth system models (ESMs) that represent permafrost processes, warming climate from anthropogenic GHG emissions deepens the active layer and enhances the decomposition of permafrost carbon, contributing to a positive carbon–climate feedback^{10,11} (although some models indicate that the concurrent increases in growing season length, nutrient mineralization, and CO₂ fixation by means of photosynthesis and storage may offset some of the carbon losses from soils^{12,13}).

While the response of decomposition to permafrost thaw is thought to be a primary mechanism for carbon release from the Arctic tundra and northern taiga¹⁴, the impact of climate change on wildfire is also recognized as an important driver^{15–19}. Lightning-triggered fires in the Arctic tundra, for example, can emit as much carbon per unit area to the atmosphere as boreal forest fires²⁰ and may drive the expansion of shrubs during post-fire successional stages^{21,22}. Fires in tundra remove moss and surface organic soil layers, allowing for greater absorption of solar radiation and thus heat flows into deeper soil layers^{20,23}. As a result, soil temperature and active layer depths increase for many years after fire, contributing to enhanced soil decomposition²⁴. The removal of surface organic soil layers also influences the plant competitive balance, with high-severity fires increasing nutrient and moisture availability in ways that favour the establishment and growth of deciduous trees^{25,26}.

Although satellite observations indicate that fire is relatively rare in the Arctic tundra and northern boreal forests near the treeline^{27,28}, several lines of evidence suggest that climate change may be increasing fire activity^{15,17}. In high-latitude North America, for example, two recent large fire years were driven by an unusually high number of lightning ignitions, many of which occurred near or at the northern treeline²⁹. Since most fires in tundra and taiga ecosystems are ignition limited, any change in lightning activity has the potential to considerably modify the fire regime³⁰. In this context, an improved understanding of the response of lightning to climate change is needed to better quantify fire threats to ecosystem function and permafrost carbon.

Lightning occurs frequently in Earth's atmosphere, with nearly 1.4 billion flashes detected each year globally²⁷. Because lightning is strongly linked to the microphysics and dynamics of thunderstorms^{31,32}, the distribution of lightning around the globe is closely linked with meteorological controls on convection^{27,33}. Many observations and modelling studies have demonstrated that lightning responds positively to surface temperature, on different temporal and spatial scales^{31,34,35}. However, this dependence on temperature does not necessarily lead to predictions of large lightning increases in response to future climate warming^{31,32}. Since the charging process of lightning is influenced mainly by the motion of ice particles within a storm, future lightning also depends on the changes in the vertical temperature profile of the atmosphere and processes influencing convection. Physically based meteorological proxies for lightning have recently been developed from observed climate–lightning relationships and have been used to predict lightning changes for future emissions pathways^{36–39}. These studies show substantial spatial heterogeneity in lightning projections. Despite improved understanding of the physical mechanisms controlling lightning, limited work has explored how the spatial and temporal patterns of lightning will evolve with climate change at high northern latitudes, as this region is not thought to be lightning rich, as

¹Department of Earth System Science, University of California, Irvine, CA, USA. ²Department of Earth and Planetary Science, University of California, Berkeley, CA, USA. ³Earth and Environmental Sciences, Lawrence Berkeley National Laboratory, Berkeley, CA, USA. ⁴Faculty of Science, Vrije Universiteit Amsterdam, Amsterdam, The Netherlands. ⁵Present address: Harvard University Center for the Environment, Harvard University, Cambridge, MA, USA. ✉e-mail: yang.chen@uci.edu

Table 1 | Contemporary and projected future lightning flash rates and associated climate and land-surface parameters

(a) Present-day mean												
Variable	Whole circumpolar high-northern-latitude region			Arctic tundra			Boreal forest			Circumpolar mean weighted by permafrost soil carbon		
	All	NA	EA	All	NA	EA	All	NA	EA	All	NA	EA
CAPE (J kg ⁻¹)	31.6	24.0	34.8	12.9	14.0	12.4	42.5	30.6	47.2	24.6	25.5	24.3
Precip (mm day ⁻¹)	2.01	1.98	2.01	1.56	1.61	1.54	2.26	2.23	2.28	1.79	1.79	1.79
CAPE×Precip (10 ⁻³ W m ⁻²)	2.46	1.88	2.71	1.03	1.08	1.01	3.30	2.42	3.64	1.93	1.90	1.93
Flash rate (number per km ² per month)	0.23	0.14	0.27	0.07	0.05	0.08	0.33	0.20	0.38	0.18	0.16	0.19
Permafrost soil carbon (kg m ⁻²)	24.6	17.5	28.6	25.6	16.0	30.2	23.8	18.6	27.1	34.4	33.9	34.6
Burned area (% yr ⁻¹)	0.27	0.32	0.24	0.09	0.05	0.11	0.37	0.50	0.32	0.28	0.36	0.25
(b) Future change relative to present-day mean (%)												
Variable	Whole circumpolar high-northern-latitude region			Arctic tundra			Boreal forest			Circumpolar mean weighted by permafrost soil carbon		
	All	NA	EA	All	NA	EA	All	NA	EA	All	NA	EA
CAPE	74 ± 15	63 ± 16	79 ± 16	100 ± 35	72 ± 23	114 ± 45	70 ± 13	60 ± 14	74 ± 14	86 ± 22	65 ± 17	93 ± 25
Precip	16 ± 1	17 ± 1	15 ± 1	20 ± 2	21 ± 2	20 ± 2	14 ± 1	15 ± 1	13 ± 1	17 ± 2	18 ± 2	17 ± 2
CAPE×Precip	90 ± 25	78 ± 21	95 ± 29	136 ± 61	98 ± 36	158 ± 82	83 ± 21	74 ± 18	87 ± 24	106 ± 35	80 ± 23	116 ± 43
Flash rate	93 ± 27	82 ± 23	99 ± 31	149 ± 72	105 ± 40	175 ± 99	85 ± 23	76 ± 20	90 ± 25	112 ± 38	84 ± 25	124 ± 48
From CAPE change	76 ± 16	64 ± 16	80 ± 16	106 ± 38	72 ± 24	123 ± 50	72 ± 14	61 ± 15	76 ± 14	89 ± 22	66 ± 17	97 ± 25
From Precip change	13 ± 1	15 ± 1	13 ± 1	20 ± 3	21 ± 2	20 ± 3	12 ± 1	13 ± 1	12 ± 1	16 ± 2	16 ± 2	16 ± 2

The table summarizes the present-day regional mean (a) and percent change by the end of the twenty-first century (b) for lightning flash rate and associated climate and land parameters during summer (May–August) in circumpolar high-northern-latitude tundra and forest. NA, North America; EA, Eurasia. The present-day climate parameters (CAPE, Precip and CAPE×Precip) are from ERA5 reanalysis (averaged over 1996–1999). The flash rate, permafrost soil carbon and burned area are from the OTD, Global Fire Emissions Database and Northern Circumpolar Soil Carbon Database, respectively. The percent changes represent the model simulated changes from a contemporary period (1986–2005) to a century-end period (2081–2100). Mean and one-standard-deviation values from an ensemble of 15 CMIP5 models are reported.

a consequence of low surface air temperatures and relatively high levels of atmospheric stability.

In this study, we estimated future changes in lightning activity across the circumpolar Arctic tundra and boreal forest region in response to global warming during the twenty-first century. We first analysed the spatial patterns of satellite lightning observations during boreal summer (taken here as May–August) of a contemporary period (1996–1999). We used a lightning flash rate product derived from the Optical Transient Detector (OTD)²⁷, a satellite remote-sensing instrument specifically designed for lightning measurements. On average, the lightning flash rate over the northern circumpolar region is substantially lower than that recorded over tropical and temperate terrestrial ecosystems²⁸. The lowest flash rates occur in Arctic tundra ecosystems (Table 1 and Extended Data Fig. 1). Contemporary flash rates in these ecosystems are a small fraction of those in North American and Eurasian boreal forests farther south. Nevertheless, climate change is accelerating faster in the Arctic than in other regions, and future changes in the lightning regime in this biome may trigger unexpected feedback with vegetation dynamics, soil thermal and active layer dynamics, hydrology, and soil CO₂ emissions.

Climate influence on the spatial pattern of summer lightning

The circumpolar spatial pattern of present-day lightning (Extended Data Fig. 1) in northern high-latitude regions closely tracks summer climate (Extended Data Fig. 2), with warmer air and stronger convection driving more lightning occurrence. By comparing flash

rate observations with ERA5 reanalysis meteorological indicators during the summers of 1996–1999, we developed a series of statistical models (Fig. 1) that reproduced the spatial variability of summer flash rates at high latitudes. We then used these relationships with changes in climate simulated by 15 Climate Model Intercomparison Project Phase 5 (CMIP5) models (Supplementary Table 1) to develop future lightning projections. Different climate proxies, including cloud top height⁴⁰, temperature⁴¹, precipitation⁴², convective mass flux⁴³ and ice flux³⁸, have been used to explain or model lightning flash rate. Here we followed the relationship between lightning flashes and the product of convective available potential energy (CAPE) and precipitation (Precip) developed by Romps et al.³⁶. To capture the full spectrum of this relationship in our study domain (that is, north of 55°N), which ranges from cold, high-latitude regions to relatively warmer boreal forest ecosystems, we also explored nonlinear regression models (Supplementary Table 2). Among different regression models that use CAPE×Precip as a predictor, the estimated flash rates from the non-parametric model (see Methods for the details) have the highest correlation with observations, while the power-law-based regressions have the best overall performance (lower biases and root mean square errors) over Arctic tundra. An arithmetic average of these models reproduces the spatial variations of summertime flash rate in the boreal forest and Arctic tundra ($R^2=0.66$) (Supplementary Table 2), making it a suitable model for estimating future changes of lightning in northern high-latitude regions.

By the end of the century for the RCP8.5 scenario, CMIP5 models project an increase in both CAPE and Precip for most areas in

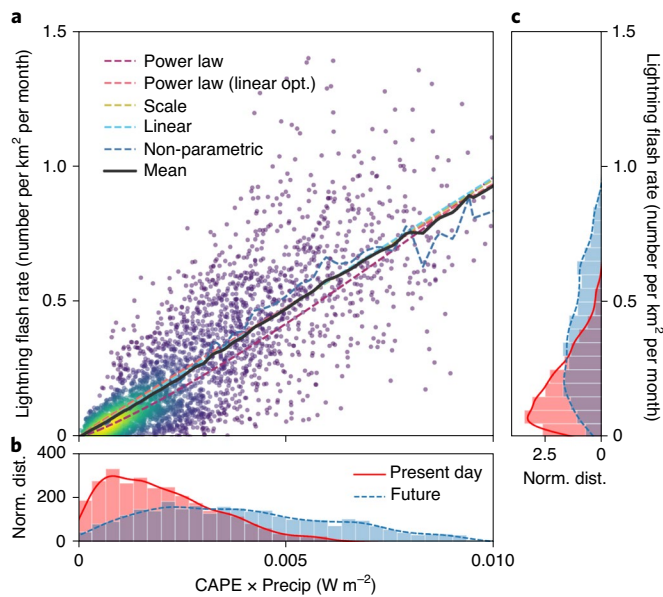


Fig. 1 | Contemporary lightning flash rates across high-northern-latitude regions are positively correlated with the product of CAPE and Precip.

a, Different statistical models derived from the spatial relationship between the present-day lightning flash rate and the product of CAPE and Precip during boreal summer (averaged over May–August of 1996–1999). Each dot represents the mean flash rate detected by the OTD and CAPE \times Precip derived from the ERA5 reanalysis over a $1^\circ \times 1^\circ$ grid cell. **b,c**, Normalized probability distributions (Norm. dist.) of CAPE \times Precip (**b**) and flash rate (**c**) for the present day (red, 1986–2005) and for the end of this century (blue, 2081–2100). The histograms of CAPE \times Precip were based on the ensemble mean of 15 CMIP5 model simulations, after applying a scaling coefficient to each model to account for different CAPE algorithms in the models and ERA5 reanalysis.

boreal forest and tundra biomes (Fig. 2a,b). CAPE is expected to increase by $100 \pm 35\%$ over Arctic tundra and by $70 \pm 13\%$ over boreal forests from the ensemble of 15 CMIP5 model simulations (Table 1). Precip is also expected to increase, although with lower levels of relative change (a $20 \pm 2\%$ increase in Arctic tundra and a $14 \pm 1\%$ increase in boreal forests). By combining these projections with the flash rate parameterization derived from contemporary measurements, we estimate that the lightning flash rate will increase by $149 \pm 72\%$ in Arctic tundra and by $85 \pm 23\%$ in boreal forests. In areas underlain with permafrost, which includes regions with both Arctic tundra and boreal forest ecosystems, the lightning flash rate is projected to increase by $112 \pm 38\%$. Increases in flash rates are relatively larger in Eurasia than in North America (Table 1), and the relative increase for Alaska ($80 \pm 22\%$) is slightly lower than that reported in a recent regional atmospheric modelling study³⁹ using boundary conditions from two different climate model simulations of future change (103% and 125%, respectively).

Changes in both CAPE and Precip contribute to the projected increase in lightning, although the role of CAPE is about five times larger because of its stronger response to climate change (Table 1). CAPE has a nonlinear dependence on surface air temperature that increases its sensitivity to polar amplification (Extended Data Fig. 3). Model-to-model differences in projected changes in CAPE and Precip are considerable in the CMIP5 ensemble (Extended Data Fig. 4) and contribute more to our uncertainty estimates reported in Table 1 than does variability introduced by the use of different statistical models relating flash rate to CAPE \times Precip (Extended Data Fig. 5).

The lightning flash rate and its future change show important variations along ecotonal gradients—specifically, across the transitional area between boreal forest and Arctic tundra ecosystems (Fig. 3). For regions north of the treeline, low present-day flash rates were observed by satellite and simulated by CMIP5 climate models. However, by the end of this century, flash rates will have a twofold to threefold increase in this region (Fig. 3a). The century-end flash rate near the treeline is predicted to be about 0.21 flashes per km^2 per month, similar to what is now detected about 480 km south of the treeline (where burned area is considerably higher). As expected, the projected changes in lightning as a function of distance to the treeline are consistent with projected changes in CAPE and Precip (Fig. 3b). Relative changes in CAPE and Precip north of the treeline (where Arctic tundra is the major biome) are substantially higher than changes south of the treeline (where boreal forest is the major biome). Modelled convective and large-scale Precip rates show increasing trends, but the percentage change of convective Precip in areas north of the treeline is substantially larger in magnitude (more than twice that for total Precip) (Extended Data Fig. 6), highlighting the importance of strengthening atmospheric convection in the Arctic.

Our results suggest that for every 1°C of global warming (using a global mean surface temperature increase of 3.7°C from the RCP8.5 scenario⁴⁴), the summer lightning flash rate will increase by $40 \pm 19\%$ in Arctic tundra, $23 \pm 6\%$ in boreal forest and $25 \pm 7\%$ in the whole circumpolar high-northern-latitude region. These sensitivities to climate warming are substantially higher than the estimates over the contiguous United States (about 12% per $^\circ\text{C}$) derived using a similar CAPE \times Precip approach³⁶, and globally (5–7% per $^\circ\text{C}$) as reported by many earlier studies using other lightning proxies^{34,45,46}. Even after adjusting for polar amplification effects on local summer surface air temperature, our estimates for relative increases in lightning across Arctic tundra are about three times as large as the previous estimates for the contiguous United States³⁶, highlighting the large changes in atmospheric stability expected at high northern latitudes.

Finney et al.³⁸ recently suggested that a decrease in cloud ice content under global warming may reduce the ice–graupel collisions necessary for cloud electrification and the formation of lightning, more than offsetting the increasing effect due to enhanced convection. This effect explained the predicted decrease in the tropics, yet their approach estimated moderate increases in lightning in high-northern-latitude regions. Romps³⁷ compared these two schemes (CAPE \times Precip and ice flux) and found that they produced similar changes in lightning over the United States. By analysing ice water path (IWP) simulated by the CMIP5 models, we find that IWP in northern high-latitude regions will also decrease in the future, but by a much smaller amount than the estimate by Finney et al.³⁸ for the tropics. Specifically, over tundra ecosystems, the mean relative decrease in IWP is only about 2%, nearly two orders of magnitude smaller than projected increases in CAPE \times Precip (Extended Data Fig. 7). On the basis of the results here, we conclude that in the high-northern-latitude regions, the dynamical response (stronger convection) will dominate the microphysical response (smaller number of ice particles) in determining lightning changes in response to future warming.

Implications for terrestrial ecosystems

Despite the rare presence of summer lightning in the present-day Arctic, the large increase in flash rate in a warming climate may initiate a series of processes and feedback pathways that amplify the impacts of climate change in terrestrial ecosystems. We hypothesize that a major pathway will be through the impact of changing lightning on wildfire occurrence. While the majority of global wildfires are intentionally or accidentally set by humans, lightning is a pre-dominant source of burning in many boreal and Arctic regions²⁹.

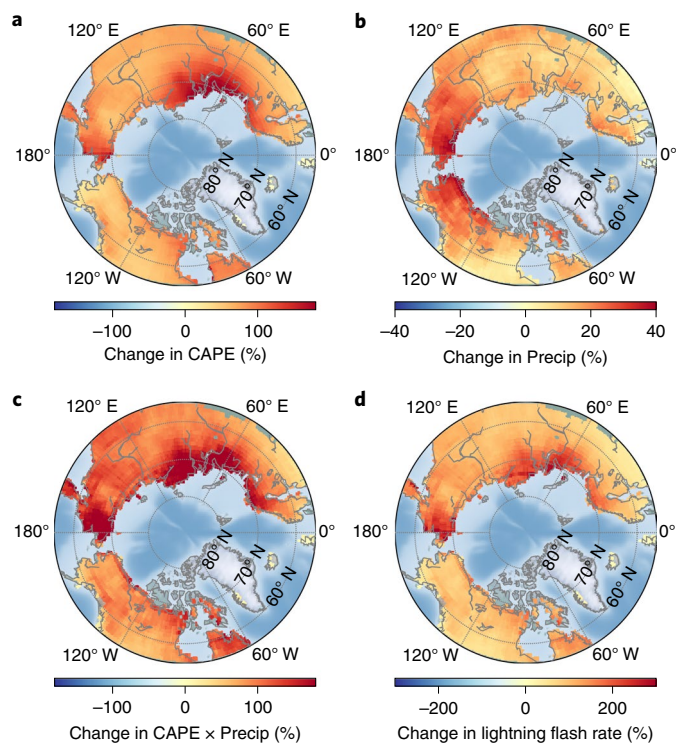


Fig. 2 | Lightning flash rates in high-northern-latitude terrestrial ecosystems are projected to increase by $93 \pm 27\%$, with a larger increase ($112 \pm 38\%$) in areas underlain by permafrost. a–d, Percentage change in summer CAPE (a), Precip (b), CAPE x Precip (c) and the lightning flash rate (d) at the end of this century (2081–2100) relative to a 1986–2005 baseline for land regions north of 55°N . These estimates represent the mean percent change for the May–August period.

Locations with more lightning often experience a higher number of fires⁴⁷. As a consequence of decreasing lightning ignition and fewer trees in more northern taiga regions near and across the boreal treeline, historical burned area shows a similar decreasing pattern (Fig. 3c and Extended Data Fig. 1d), with very few tundra fires observed during the satellite era¹⁷. By analysing observed fire perimeters for Alaska⁴⁸ and Canada⁴⁹, we find that the latitudinal burned area gradient over boreal forests near (within 500 km of) the treeline is closely associated with decreasing fire number (Extended Data Fig. 8b,c). Mean fire size, in contrast, shows a more variable relationship, decreasing towards the treeline in Alaska but showing a weaker dependency on latitude in Canada. For the contemporary climate, less than 0.05% of the Arctic tundra area (within 500 km north of the treeline) burns each year, a level that is about ten times lower than that observed in dense interior boreal forest regions farther to the south (Fig. 3c). The spatial structure of the fire observations and the differences between fire number and size as functions of distance to treeline suggest that lightning-driven fire starts are a primary limit to annual burned area levels near and across the treeline, and within Arctic tundra. To estimate burned area from the changes in flash rate, we computed a ratio of burned area to flash rate using contemporary burned area and lightning observations. This ratio is considerably higher in boreal forests and integrates a series of vegetation and climate controls on fire occurrence and fire size (Extended Data Fig. 8a). Notably, the low live-fuel moisture of needles and ladder fuels of black spruce trees (*Picea mariana*) may enhance ignition probabilities and fire spread⁵⁰, yielding a higher efficacy of lightning strikes to burned area in interior boreal forests. We estimated future changes in burned area assuming that this ratio will remain the same in each latitude band (referred to as the

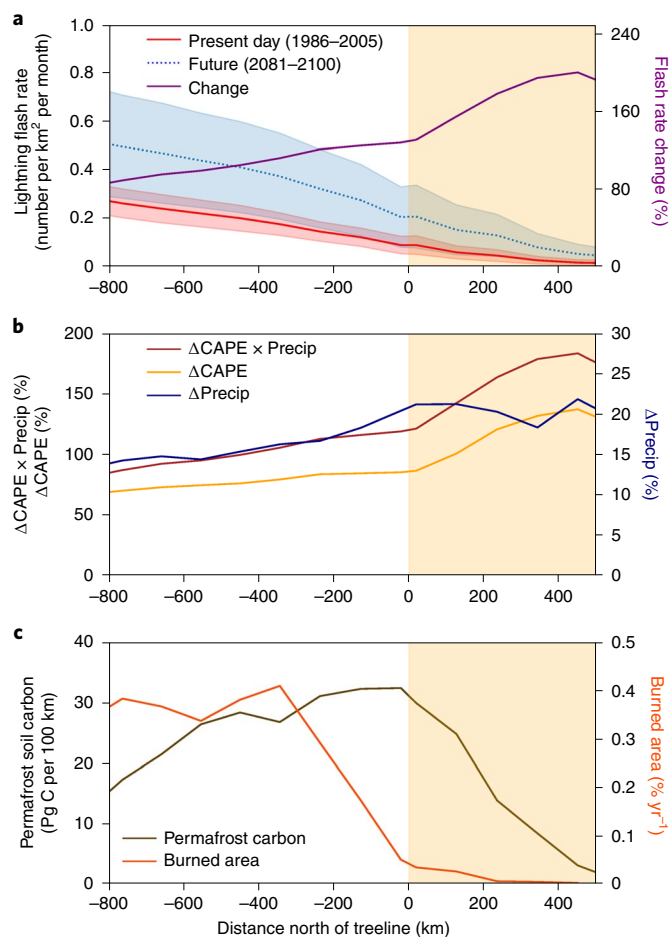


Fig. 3 | By the end of the twenty-first century, projected lightning flash rates over Arctic tundra are similar to levels now detected over boreal forests south of the treeline. a, Flash rate distributions in the present day (red) and for the end of the twenty-first century (blue) as a function of distance from the northern treeline (positive values indicate north of the treeline). The lines and shading represent the means and one-standard-deviation ranges from 15 CMIP5 models and 5 statistical models relating flash rate to CAPE x Precip. The purple line represents the percent change in flash rate. b, The percent changes in CAPE, Precip and their product by the end of this century. c, The distributions of present-day permafrost soil carbon to a depth of 100 cm and present-day annual burned area. The orange shading indicates the Arctic tundra region within 500 km of the northern treeline.

‘static vegetation’ approach), acknowledging that this approach is overly simplified. We estimated an increase of $158 \pm 96\%$ in burned area (from 459 to $1,184 \text{ km}^2 \text{ yr}^{-1}$) and CO_2 emissions (from 0.93 to $2.39 \text{ Tg C yr}^{-1}$) over vulnerable Arctic tundra by the end of the twenty-first century (Supplementary Table 3).

Lightning-driven increases in fire may trigger a positive fire–vegetation–soil feedback that promotes shrub expansion, northward displacement of the treeline and changes in tree species composition^{8,25,51,52}. A dynamic vegetation feedback may develop over a longer timescale than the atmospheric processes that regulate lightning flash rate and fire ignition. Palaeorecords provide evidence in some regions that shrub-dominant tundra can sustain a higher fire frequency than what is currently observed during the satellite era³³. With more lightning-driven ignition, we expect more fire occurrence in taiga ecosystems at or above the northern treeline by year 2100 (Fig. 4a). Losses of moss and surface duff layers in fire-affected

areas, in turn, are likely to promote permafrost thaw and the establishment of more trees (which need access to larger reservoirs of surface soil moisture and nutrients during the growing season^{54,55}) and fire-tolerant shrub species in nearby tundra^{21,56}.

Several important feedback pathways can arise from these vegetation changes. First, more shrubs and trees may enhance local lightning storm development by increasing surface sensible heat fluxes⁵⁷. Second, as described above, evergreen conifer forests in North America provide fuels that are more flammable and thus more likely to promote crown fires, allowing for higher levels of fuel continuity and larger fire sizes. Both factors may facilitate increases in fire occurrence and burned area, which in turn enhances the establishment of shrubs and trees. At the same time, vapour pressure deficit is expected to increase, and differences between Precip and evapotranspiration are expected to remain nearly the same (Extended Data Fig. 9), providing evidence that climate change may cause drying of dead fine fuels. Vapour pressure deficit is known to structure fire occurrence, fire size and other aspects of fire dynamics in contemporary boreal forests⁵⁸. Together, the vegetation dynamics and changes in fire weather may contribute to a higher ratio of burned area to lightning flash rate north of the treeline than what is currently observed (Extended Data Fig. 8a). After we add this amplifying effect from a vegetation feedback into our simple fire model (by assuming that the ratio of burned area to lightning flash rate in the Arctic tundra will change to the present-day value in boreal forests 480 km south of the treeline, referred to as the 'dynamic vegetation' approach), the model predicts a $570 \pm 480\%$ enhancement in burned area and carbon release by the end of this century in Arctic tundra.

Increases in burned area within Arctic tundra, in turn, may increase the vulnerability of the permafrost carbon reservoir in at least two ways (Fig. 4b). First, more frequent fires have the potential to damage or remove the surface insulating layer of organic matter in areas that have moderate or high fire severity⁵⁹. The loss of this layer through wildfire combustion will expose the underlying permafrost to substantial warming and degradation⁸ and lead to thermokarst development in ice-rich permafrost⁶⁰. Permafrost degradation has begun in some high-northern-latitude regions⁶¹ and is likely to accelerate the permafrost-carbon-climate feedback with further warming^{6,62}, increase the probability of abrupt permafrost thaw⁷ and potentially alter the trajectory of global climate change. Second, with the expansion of shrubs and northern forests in fire-disturbed areas, surface albedo will probably decline in spring and summer, and the extra energy absorbed by the land surface may further amplify regional climate warming⁶³. Decreases in surface albedo are expected from evergreen conifer trees shielding snow-covered surfaces during spring, from darker foliage (in the case of conifers) reducing visible and near-infrared reflectance during summer²³, and from the deposition of black carbon on nearby sea ice and land ice surfaces⁶⁴. Summer evapotranspiration rates may also increase from increasing forest cover, trapping outgoing longwave radiation⁶⁵. Increases in fine root biomass associated with shrub and tree expansion may additionally stimulate the decomposition of permafrost soil carbon through rhizosphere priming⁶⁶. Extra warming and productivity from a fire-driven northward expansion of forests could thus accelerate permafrost thaw and decomposition in areas not currently affected by fire.

Discussion and conclusions

These results highlight the need for modelling fire dynamics in ESMs that simulate coupled biogeochemical cycles at northern high latitudes⁶⁷. Lightning has been included in most state-of-the-art ESMs for the purpose of simulating atmospheric chemistry and fire ignition⁶⁸, but responses of lightning to climate change have been challenging to quantify with existing modelling frameworks. For example, the lightning parameterizations used in many of these

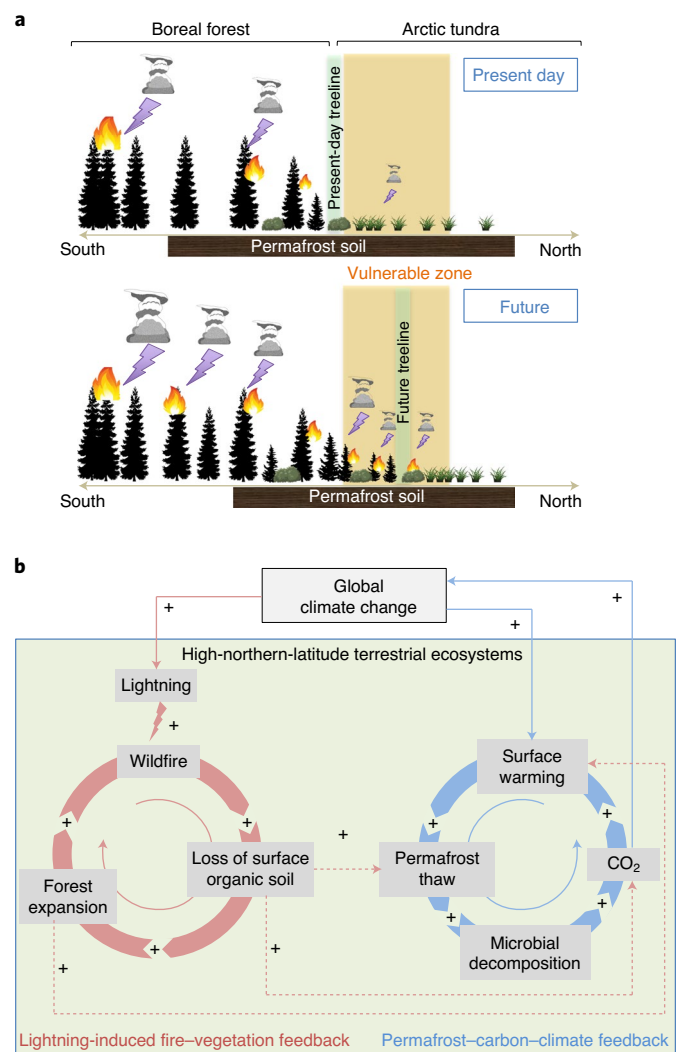


Fig. 4 | Future increases in lightning flash rate may initiate a feedback that amplifies the impacts of climate change in high-northern-latitude terrestrial ecosystems. **a**, In a warming climate, lightning increases may cause more lightning-ignited fires and thereby accelerate forest expansion and the poleward advance of the treeline. The northern expansion of trees, in turn, may contribute to additional warming. **b**, Schematic illustration of how lightning-induced fire-vegetation interactions may amplify the permafrost-carbon-climate feedback in taiga and Arctic tundra ecosystems. The dashed lines highlight the pathways through which the lightning-fire-vegetation feedback loop influences the permafrost-carbon-climate feedback loop. While the expansion of forests north of the treeline may lead to increases in aboveground carbon stocks, losses from belowground pools are expected to be much larger, yielding a net loss of carbon from the ecosystem. The lightning-driven increases in forest area at the treeline shown in **a** are expected to amplify warming from albedo and land surface fluxes^{75,76}.

models^{40,43} were derived from temperate and tropical observations and may not be applicable to high-latitude regions. Lightning occurrence in the Arctic is a small contributor to global patterns and is thus prone to biases in global-scale parameterizations, which in turn could notably influence the simulation of tundra fires in current ESMs^{30,69}. Because lightning is currently rare in Arctic tundra ecosystems, the large projected changes we identify here have the potential to considerably modify vegetation dynamics and the carbon balance of Arctic ecosystems. Future experiments with climate

models need to include these responses and feedback pathways to improve the analysis of vulnerability, impacts and adaptation and to reduce uncertainties in future projections of other aspects of the Earth system.

Modern advances in remote-sensing technology have provided unprecedented opportunities to precisely locate lightning occurrences in tropical and temperate regions²⁸. Previous lightning detections in the Arctic, however, seem inadequate for long-term trend detection. The OTD measurements used in this study provided an internally consistent set of estimates that are relatively insensitive to sampling issues associated with ground-based detector networks. However, the OTD instrument was retired two decades ago, and no satellite replacement is currently available in a low Earth orbit. Follow-up lightning missions, including Lightning Imaging Sensors (LIS; onboard the Tropical Rainfall Measuring Mission and the International Space Station) and Global Lightning Mapper (onboard GOES-16), despite their higher sensitivity and temporal coverage, primarily detect lightning in tropical and midlatitude regions. Surface-based lightning observation networks, such as the North American Lightning Detection Network⁷⁰, World Wide Lightning Location Network⁷¹ and Global Lightning Dataset⁷², have expanded in coverage and sensitivity, yet the evolution of detectors and network structure may pose challenges for long-term trend analysis. Since future warming in the Arctic is expected to be higher than the global mean⁷³, the accurate projection of future lightning changes will need consistent high-quality lightning observations from space and ground-based networks. Such measurements are essential for quantitatively understanding both the drivers and the impacts of a changing lightning regime in the Arctic.

Climate warming and polar amplification⁷⁴ contribute to the thawing permafrost and the decomposition of ancient soil organic material. These changes increase the probability of abrupt thaw and collapse⁷ and a positive feedback with atmospheric CO₂. In this study, we describe a lightning–fire–vegetation feedback pathway that may interact with and accelerate the permafrost–carbon–climate feedback. We show that climate change may significantly increase lightning density in northern circumpolar regions, leading to a shift in fire regimes and vegetation composition, as well as additional warming. Given the large amount of permafrost soil carbon stored in northern ecosystems, this analysis highlights the importance of improving lightning monitoring in the Arctic and the need to develop better models of lightning, fire dynamics and feedback with vegetation and soils.

Online content

Any methods, additional references, Nature Research reporting summaries, source data, extended data, supplementary information, acknowledgements, peer review information; details of author contributions and competing interests; and statements of data and code availability are available at <https://doi.org/10.1038/s41558-021-01011-y>.

Received: 14 August 2020; Accepted: 17 February 2021;

Published online: 5 April 2021

References

- Hugelius, G. et al. Estimated stocks of circumpolar permafrost carbon with quantified uncertainty ranges and identified data gaps. *Biogeosciences* **11**, 6573–6593 (2014).
- Mishra, U. et al. Empirical estimates to reduce modeling uncertainties of soil organic carbon in permafrost regions: a review of recent progress and remaining challenges. *Environ. Res. Lett.* <https://doi.org/10.1088/1748-9326/8/3/035020> (2013).
- Scharlemann, J. P. W., Tanner, E. V. J., Hiederer, R. & Kapos, V. Global soil carbon: understanding and managing the largest terrestrial carbon pool. *Carbon Manage.* **5**, 81–91 (2014).
- Pan, Y. D. et al. A large and persistent carbon sink in the world's forests. *Science* **333**, 988–993 (2011).
- Hugelius, G. et al. The Northern Circumpolar Soil Carbon Database: spatially distributed datasets of soil coverage and soil carbon storage in the northern permafrost regions. *Earth Syst. Sci. Data* **5**, 3–13 (2013).
- Schuur, E. A. G. et al. Climate change and the permafrost carbon feedback. *Nature* **520**, 171–179 (2015).
- Turetsky, M. R. et al. Carbon release through abrupt permafrost thaw. *Nat. Geosci.* **13**, 138–143 (2020).
- McGuire, A. D. et al. Sensitivity of the carbon cycle in the Arctic to climate change. *Ecol. Monogr.* **79**, 523–555 (2009).
- Strauss, J. et al. Deep Yedoma permafrost: a synthesis of depositional characteristics and carbon vulnerability. *Earth Sci. Rev.* **172**, 75–86 (2017).
- Koven, C. D., Lawrence, D. M. & Riley, W. J. Permafrost carbon–climate feedback is sensitive to deep soil carbon decomposability but not deep soil nitrogen dynamics. *Proc. Natl Acad. Sci. USA* **112**, 3752–3757 (2015).
- Lawrence, D. M., Koven, C. D., Swenson, S. C., Riley, W. J. & Slater, A. G. Permafrost thaw and resulting soil moisture changes regulate projected high-latitude CO₂ and CH₄ emissions. *Environ. Res. Lett.* **10**, 094011 (2015).
- McGuire, A. D. et al. Dependence of the evolution of carbon dynamics in the northern permafrost region on the trajectory of climate change. *Proc. Natl Acad. Sci. USA* **115**, 3882–3887 (2018).
- Mekonnen, Z. A., Riley, W. J. & Grant, R. F. 21st century tundra shrubification could enhance net carbon uptake of North America Arctic tundra under an RCP8.5 climate trajectory. *Environ. Res. Lett.* <https://doi.org/10.1088/1748-9326/aabf28> (2018).
- Skädel, C. et al. Potential carbon emissions dominated by carbon dioxide from thawed permafrost soils. *Nat. Clim. Change* **6**, 950–953 (2016).
- Turetsky, M. R. et al. Recent acceleration of biomass burning and carbon losses in Alaskan forests and peatlands. *Nat. Geosci.* **4**, 27–31 (2011).
- Veraverbeke, S., Rogers, B. M. & Randerson, J. T. Daily burned area and carbon emissions from boreal fires in Alaska. *Biogeosciences* **12**, 3579–3601 (2015).
- Hu, F. S. et al. Arctic tundra fires: natural variability and responses to climate change. *Front. Ecol. Environ.* **13**, 369–377 (2015).
- Rogers, B. M., Balch, J. K., Goetz, S. J., Lehmann, C. E. R. & Turetsky, M. Focus on changing fire regimes: interactions with climate, ecosystems, and society. *Environ. Res. Lett.* <https://doi.org/10.1088/1748-9326/ab6d3a> (2020).
- Walker, X. J. et al. Increasing wildfires threaten historic carbon sink of boreal forest soils. *Nature* **572**, 520–523 (2019).
- Mack, M. C. et al. Carbon loss from an unprecedented Arctic tundra wildfire. *Nature* **475**, 489–492 (2011).
- Harsch, M. A., Hulme, P. E., McGlone, M. S. & Duncan, R. P. Are treelines advancing? A global meta-analysis of treeline response to climate warming. *Ecol. Lett.* **12**, 1040–1049 (2009).
- Rocha, A. V. et al. The footprint of Alaskan tundra fires during the past half-century: implications for surface properties and radiative forcing. *Environ. Res. Lett.* **7**, 044039 (2012).
- Chambers, S. D., Beringer, J., Randerson, J. T. & Chapin, F. S. III Fire effects on net radiation and energy partitioning: contrasting responses of tundra and boreal forest ecosystems. *J. Geophys. Res. Atmos.* <https://doi.org/10.1029/2004jd005299> (2005).
- Genet, H. et al. Modeling the effects of fire severity and climate warming on active layer thickness and soil carbon storage of black spruce forests across the landscape in interior Alaska. *Environ. Res. Lett.* **8**, 045016 (2013).
- Mekonnen, Z. A., Riley, W. J., Randerson, J. T., Grant, R. F. & Rogers, B. M. Expansion of high-latitude deciduous forests driven by interactions between climate warming and fire. *Nat. Plants* **5**, 952–958 (2019).
- Johnstone, J. F., Hollingworth, T. N., Chapin, F. S. III & Mack, M. C. Changes in fire regime break the legacy lock on successional trajectories in Alaskan boreal forest. *Glob. Change Biol.* **16**, 1281–1295 (2010).
- Christian, H. J. et al. Global frequency and distribution of lightning as observed from space by the Optical Transient Detector. *J. Geophys. Res. Atmos.* <https://doi.org/10.1029/2002jd002347> (2003).
- Cecil, D. J., Buechler, D. E. & Blakeslee, R. J. Gridded lightning climatology from TRMM-LIS and OTD: dataset description. *Atmos. Res.* **135**, 404–414 (2014).
- Veraverbeke, S. et al. Lightning as a major driver of recent large fire years in North American boreal forests. *Nat. Clim. Change* **7**, 529–534 (2017).
- Krause, A., Kloster, S., Wilkenskjaeld, S. & Paeth, H. The sensitivity of global wildfires to simulated past, present, and future lightning frequency. *J. Geophys. Res. Biogeosci.* **119**, 312–322 (2014).
- Price, C. Lightning applications in weather and climate research. *Surv. Geophys.* **34**, 755–767 (2013).
- Williams, E. R. Lightning and climate: a review. *Atmos. Res.* **76**, 272–287 (2005).
- Albrecht, R. I., Goodman, S. J., Buechler, D. E., Blakeslee, R. J. & Christian, H. J. Where are the lightning hotspots on Earth? *Bull. Am. Meteorol. Soc.* **97**, 2051–2068 (2016).

34. Price, C. & Rind, D. Possible implications of global climate change on global lightning distributions and frequencies. *J. Geophys. Res. Atmos.* **99**, 10823–10831 (1994).
35. Jayaratne, E. R. & Kuleshov, Y. The relationship between lightning activity and surface wet bulb temperature and its variation with latitude in Australia. *Meteorol. Atmos. Phys.* **91**, 17–24 (2006).
36. Roms, D. M., Seeley, J. T., Vollaro, D. & Molinari, J. Projected increase in lightning strikes in the United States due to global warming. *Science* **346**, 851–854 (2014).
37. Roms, D. M. Evaluating the future of lightning in cloud-resolving models. *Geophys. Res. Lett.* **46**, 14863–14871 (2019).
38. Finney, D. L. et al. A projected decrease in lightning under climate change. *Nat. Clim. Change* **8**, 210–213 (2018).
39. Bieniek, P. A. et al. Lightning variability in dynamically downscaled simulations of Alaska's present and future summer climate. *J. Appl. Meteorol. Climatol.* **59**, 1139–1152 (2020).
40. Price, C. & Rind, D. A simple lightning parameterization for calculating global lightning distributions. *J. Geophys. Res. Atmos.* **97**, 9919–9933 (1992).
41. Reeve, N. & Toumi, R. Lightning activity as an indicator of climate change. *Q. J. R. Meteorol. Soc.* **125**, 893–903 (1999).
42. Petersen, W. A. & Rutledge, S. A. On the relationship between cloud-to-ground lightning and convective rainfall. *J. Geophys. Res. Atmos.* **103**, 14025–14040 (1998).
43. Allen, D. J. & Pickering, K. E. Evaluation of lightning flash rate parameterizations for use in a global chemical transport model. *J. Geophys. Res. Atmos.* **107**, ACH 15-1–ACH 15-21 (2002).
44. IPCC *Climate Change 2014: Synthesis Report* (eds Core Writing Team, Pachauri, R. K. & Meyer L. A.) (IPCC, 2014).
45. Price, C. Global surface temperatures and the atmospheric electrical circuit. *Geophys. Res. Lett.* **20**, 1363–1366 (1993).
46. Michalon, N., Nassif, A., Saouri, T., Royer, J. F. & Pontikis, C. A. Contribution to the climatological study of lightning. *Geophys. Res. Lett.* **26**, 3097–3100 (1999).
47. Peterson, D., Wang, J., Ichoku, C. & Remer, L. A. Effects of lightning and other meteorological factors on fire activity in the North American boreal forest: implications for fire weather forecasting. *Atmos. Chem. Phys.* **10**, 6873–6888 (2010).
48. Kasischke, E. S., Williams, D. & Barry, D. Analysis of the patterns of large fires in the boreal forest region of Alaska. *Int. J. Wildland Fire* **11**, 131–144 (2002).
49. Stocks, B. J. et al. Large forest fires in Canada, 1959–1997. *J. Geophys. Res. Atmos.* <https://doi.org/10.1029/2001jd000484> (2002).
50. Rogers, B. M., Soja, A. J., Goulden, M. L. & Randerson, J. T. Influence of tree species on continental differences in boreal fires and climate feedbacks. *Nat. Geosci.* **8**, 228–234 (2015).
51. McGuire, A. D., Chapin, F. S., Walsh, J. E. & Wirth, C. Integrated regional changes in Arctic climate feedbacks: implications for the global climate system. *Annu. Rev. Environ. Resour.* **31**, 61–91 (2006).
52. Euskirchen, E. S., McGuire, A. D., Chapin, F. S. III, Yi, S. & Thompson, C. C. Changes in vegetation in northern Alaska under scenarios of climate change, 2003–2100: implications for climate feedbacks. *Ecol. Appl.* **19**, 1022–1043 (2009).
53. Higuera, P. E. et al. Frequent fires in ancient shrub tundra: implications of paleorecords for Arctic environmental change. *PLoS ONE* **3**, e0001744 (2008).
54. Trugman, A. et al. Climate, soil organic layer, and nitrogen jointly drive forest development after fire in the North American boreal zone. *J. Adv. Model. Earth Syst.* **8**, 1180–1209 (2016).
55. Bret-Harte, M. S. et al. The response of Arctic vegetation and soils following an unusually severe tundra fire. *Phil. Trans. R. Soc. B* <https://doi.org/10.1098/rstb.2012.0490> (2013).
56. Turner, M. G. Disturbance and landscape dynamics in a changing world. *Ecology* **91**, 2833–2849 (2010).
57. Dissing, D. & Verbyla, D. L. Spatial patterns of lightning strikes in interior Alaska and their relations to elevation and vegetation. *Can. J. For. Res.* **33**, 770–782 (2003).
58. Sedano, F. & Randerson, J. T. Multi-scale influence of vapor pressure deficit on fire ignition and spread in boreal forest ecosystems. *Biogeosciences* **11**, 3739–3755 (2014).
59. Yi, S. H., Woo, M. K. & Arain, M. A. Impacts of peat and vegetation on permafrost degradation under climate warming. *Geophys. Res. Lett.* **34**, L16504 (2007).
60. Jones, B. M. et al. Recent Arctic tundra fire initiates widespread thermokarst development. *Sci. Rep.* <https://doi.org/10.1038/srep15865> (2015).
61. Brown, D. R. N. et al. Landscape effects of wildfire on permafrost distribution in interior Alaska derived from remote sensing. *Remote Sens.* <https://doi.org/10.3390/rs8080654> (2016).
62. Walker, G. A world melting from the top down. *Nature* **446**, 718–721 (2007).
63. Bonfils, C. J. W. et al. On the influence of shrub height and expansion on northern high latitude climate. *Environ. Res. Lett.* <https://doi.org/10.1088/1748-9326/7/1/015503> (2012).
64. McConnell, J. R. et al. 20th-century industrial black carbon emissions altered Arctic climate forcing. *Science* **317**, 1381–1384 (2007).
65. Swann, A. L., Fung, I. Y., Levis, S., Bonan, G. B. & Doney, S. C. Changes in Arctic vegetation amplify high-latitude warming through the greenhouse effect. *Proc. Natl Acad. Sci. USA* **107**, 1295–1300 (2010).
66. Keuper, F. et al. Carbon loss from northern circumpolar permafrost soils amplified by rhizosphere priming. *Nat. Geosci.* **13**, 560–565 (2020).
67. Bonan, G. B. & Doney, S. C. Climate, ecosystems, and planetary futures: the challenge to predict life in Earth system models. *Science* <https://doi.org/10.1126/science.aam8328> (2018).
68. Magi, B. I. Global lightning parameterization from CMIP5 climate model output. *J. Atmos. Ocean. Technol.* **32**, 434–452 (2015).
69. Kloster, S. & Lasslop, G. Historical and future fire occurrence (1850 to 2100) simulated in CMIP5 Earth System Models. *Glob. Planet. Change* **150**, 58–69 (2017).
70. Orville, R. E., Huffines, G. R., Burrows, W. R. & Cummins, K. L. The North American Lightning Detection Network (NALDN)—analysis of flash data: 2001–09. *Mon. Weather Rev.* **139**, 1305–1322 (2011).
71. Virts, K. S., Wallace, J. M., Hutchins, M. L. & Holzworth, R. H. Highlights of a new ground-based, hourly global lightning climatology. *Bull. Am. Meteorol. Soc.* **94**, 1381–1391 (2013).
72. Pohjola, H. & Makela, A. The comparison of GLD360 and EUCLID lightning location systems in Europe. *Atmos. Res.* **123**, 117–128 (2013).
73. Collins, M. et al. in *Climate Change 2013: The Physical Science Basis* (eds Stocker, T. F. et al.) Ch. 12 (IPCC, Cambridge Univ. Press, 2013).
74. Screen, J. A. & Simmonds, I. The central role of diminishing sea ice in recent Arctic temperature amplification. *Nature* **464**, 1334–1337 (2010).
75. Chapin, F. S. et al. Role of land-surface changes in Arctic summer warming. *Science* **310**, 657–660 (2005).
76. Foley, J. A. Tipping points in the tundra. *Science* **310**, 627–628 (2005).

Publisher's note Springer Nature remains neutral with regard to jurisdictional claims in published maps and institutional affiliations.

© The Author(s), under exclusive licence to Springer Nature Limited 2021

Methods

Study region and land cover types. In this study, we focused on circumpolar boreal land north of 55°N, excluding areas that are bare or permanently covered in ice or snow. We used the Moderate Resolution Imaging Spectroradiometer (MODIS) land cover type climate modelling grid product (MCD12C1, <https://lpdaac.usgs.gov/products/mcd12c1v006/>)⁷⁷ to calculate the vegetation cover fraction (VCF) and tree cover fraction (TCF) in each 1° grid cell by summing the cover fractions at the native resolution (0.05°). All natural vegetation types (classes 1–10 in the International Geosphere–Biosphere Programme classification, excluding human-influenced land cover types such as croplands and urban area) were used to compute VCF, and all forest types (classes 1–5) were used to derive TCF. Within vegetated land area (VCF > 20%), we defined areas with TCF greater than 1% as boreal forest and areas with TCF less than 1% as Arctic tundra. We further separated the study region into two continental-scale regions: North America and Eurasia.

Lightning data. Space-borne optical lightning sensors provide a global coverage of lightning climatology in recent decades^{27,28}. The OTD on the MicroLab-1 satellite (later renamed to OV-1) was a space-based instrument specifically designed to detect and locate lightning, day and night²⁷. The 70° inclination low Earth orbit of OV-1 enabled the OTD to record lightning activity over northern high latitudes (up to 75°N). Over its nearly five-year mission (May 1995 to March 2000), the OTD monitored the occurrence of lightning and measured the radiant energy at a 10 km spatial resolution and a 2 ms temporal resolution.

Here we used the LIS/OTD merged gridded lightning climatology data product (https://lightning.nsstc.nasa.gov/data/data_lis-otd-climatology.html) provided by the NASA Global Hydrology Resource Center²⁸. On the basis of the 0.5° high-resolution monthly climatology dataset, we derived a climatological mean (representing the years of 1996–1999) of total lightning flash rate for the boreal summer (May–August) for each 1° grid cell. Previous observations provided evidence of a strong diurnal variation in lightning activity over land^{28,29}. Due to its near-polar orbit, the OTD detected lightning at different local times, with a full sampling of the diurnal cycle in 55 days^{27,41}. Our use of the whole-summer data over a four-month period minimizes the bias caused by the different overpass times in different places and in different years.

By comparing the OTD data with lightning flash rates reported by the Alaskan Lightning Detection Network (ALDN) (<https://fire.ak.blm.gov/predsvcs/maps.php>) during the same period, we found that the spatial patterns from the satellite and the ground network agree well in Alaska (Extended Data Fig. 10). The difference in magnitude was probably due to the fact that ALDN detects only cloud-to-ground lightning strikes; in addition, ALDN had lower detection efficiency and accuracy before the system upgrade in 2000 (ref. ⁸⁰).

Meteorological data. To derive a statistical model between meteorological variables and the observed lightning flash rate, we used the ERA5 global reanalysis dataset (<https://www.ecmwf.int/en/forecasts/datasets/reanalysis-datasets/era5>)⁸¹ provided by the European Centre for Medium-Range Weather Forecasts. We extracted hourly meteorological fields, including the total Precip and CAPE, at 1° × 1° resolution during boreal summers (May–August) of 1996–1999 from the original ERA5 data. We calculated the product of CAPE and Precip (CAPE × Precip) at hourly intervals and then averaged the data over summer months in each grid cell.

To create projections of lightning changes for the twenty-first century, we analysed meteorological output from 15 global climate models (GCMs) that participated in CMIP5 (<https://cmip.llnl.gov/cmip5>)⁸². A full list of CMIP5 models used in this study is shown in Supplementary Table 1. We extracted monthly Precip, the convective Precip, evapotranspiration, surface temperature, surface relative humidity and IWP from these models. We derived the vapour pressure deficit and Precip minus evapotranspiration from these monthly CMIP5 outputs.

We also diagnosed convective instability and calculated CAPE from each GCM at six-hour intervals. At the same time, we extracted Precip for the three-hour periods immediately following the six-hourly CAPE snapshots recorded at 0:00, 6:00, 12:00 and 18:00 UTC⁸³. We then calculated CAPE × Precip at these subdaily time steps and used the high-resolution time series to estimate monthly mean values. In a final step, we converted all of the CMIP5 model datasets to the spatial resolution of 1° × 1° grid cells using linear interpolation.

During the four summers with valid OTD flash rate observations (1996–1999), CAPE × Precip from the CMIP5 models has a similar spatial pattern to that from the ERA5 reanalysis (Extended Data Fig. 2c). However, since different approaches were used to calculate CAPE (ERA5 used a maximum-unstable, pseudo-adiabatic, liquid-only algorithm, while our method of estimating CAPE from the CMIP5 models was surface-based, adiabatic and included both liquid and ice phases), the absolute values of CAPE × Precip from these two data sources were different. Using the ERA5 and CMIP5 data in northern high-latitude regions during the summers of 1996–1999, we derived a single scaling coefficient (γ) for each model, so that CAPE × Precip from each model during the historical period matched the ERA5 reanalysis.

CMIP5 model estimates of climate provided a consistent pathway for predicting future change by combining information from historical and future

simulations. On the basis of monthly data from each CMIP5 model, we calculated a boreal summer (May–August) mean meteorology for two periods: a present-day period used to estimate a climatology of contemporary lightning (1986–2005) and a future period at the end of the twenty-first century (2081–2100). The future projections in our analysis were based on RCP8.5, a business-as-usual pathway of future GHG concentrations⁸⁴. By averaging data over 20-year periods for the present-day and future time intervals, we attempted to minimize the influence of internal climate variability (and climate modes) on lightning variability on shorter timescales (including, for example, linkages between the lightning occurrence and El Niño/Southern Oscillation)^{85,86}. We also analysed future changes in summer Precip, convective Precip, CAPE, surface air temperature and vapour pressure deficit to identify the relative importance of these different drivers for changes in lightning flash rate and for a broader assessment of changes in atmospheric stability and surface climate.

All meteorological data were extracted for individual CMIP5 models first, and they were then used to calculate the mean and variance for the multimodel ensemble.

Statistical models of lightning flash rate. Using mean values (averaged for the summers of 1996–1999) in 1° × 1° grid cells of northern high-latitude regions, we explored several different linear and nonlinear statistical regression models (Supplementary Table 2) between the satellite-detected lightning flash rate (FR) and CAPE × Precip from the ERA5 reanalysis.

The first model (hereafter ‘power law’) was a power law regression: $FR = a(\text{CAPE} \times \text{Precip})^b$, with the parameters a and b derived from the optimization at the log-log scale (that is, a linear regression between logarithmic values of flash rate and CAPE × Precip were performed in practice). Similar to Romps et al.³⁶, this model assumed that the lightning flash rate depends on the product of CAPE and Precip. The coefficient b allows nonlinear impacts to be represented in this form. The second model (‘power law (linear opt)’) is a variation of the power law model, but with the least squares optimization obtained without a logarithmic transformation. The third model (‘scale’) we used was the original scaling approach proposed by Romps et al.³⁶: $FR = a(\text{CAPE} \times \text{Precip})$. In the fourth model (‘linear’), we slightly modified the scaling approach by allowing a negative intercept: $FR = a(\text{CAPE} \times \text{Precip}) + b$ —that is, positive flash rate was simulated only when CAPE × Precip was greater than a threshold. In addition to these parametric approaches, we derived a non-parametric regression model (‘non-parametric’) that includes a lookup table of flash rate as a function of CAPE × Precip within the range of contemporary observations. The modelled flash rate value in each bin was derived using the arithmetic means of the observed flash rate in all grid cells associated with the corresponding ranges of CAPE × Precip. A linear extrapolation was used to extend the model to cover CAPE × Precip values outside of the observational range. We recorded the ensemble means from these five regression models (‘mean’) as our reference model for flash rate estimation.

Future projections of lightning. We combined the statistical regression models described above with gridded CAPE × Precip values from different CMIP5 GCMs to estimate the changes in summertime lightning flash rate during the twenty-first century. The mean CAPE × Precip values for a contemporary period (1986–2005) and a future period (2081–2100) were first adjusted using the scaling coefficient (γ) derived from the 1996–1999 data (‘Meteorological data’). We derived lightning flash rate estimates for each CMIP5 model by applying the different statistical models described in ‘Statistical models of lightning flash rate’ to the adjusted CAPE × Precip estimates described in ‘Meteorological data’. We reported the ensemble mean flash rate from all model estimates for both the contemporary and future periods, as well as the changes during the twenty-first century. We estimated uncertainties for our flash rate projections by combining information about model-to-model differences in projections of future climate with information regarding the use of different statistical models to relate CAPE × Precip to flash rate. This was done by separately computing the change in future flash rate predicted by each of the 15 separate CMIP5 models and by each of the 5 statistical models. This analysis yielded a set of 75 estimates, and we report the standard deviation of this set of simulations as our uncertainty estimate.

To separate contributions of CAPE and Precip to future lightning changes, we performed two additional calculations in which CAPE or Precip was assumed to be the same during the contemporary and future periods. In these two experiments, the projected lightning flash rate for the future period (2081–2100) was determined either only by the CAPE change or only by the Precip change.

Fire data. The mean annual burned area (in % per year) for each grid cell in the circumpolar boreal region was estimated from version 4s of the Global Fire Emissions Database (GFED4s, <http://www.globalfiredata.org/>)^{87,88}. GFED4s burned area after August 2000 was based on the surface reflectance and thermal anomaly observations by MODIS aboard the Terra and Aqua satellites. This burned area estimate was then extended to the pre-MODIS era using statistical relationships⁸⁸ developed between MODIS burned area and active fire detections from the European Space Agency Advanced Along Track Scanning Radiometer. The climatological averages for all years during the GFED period (1996–2016) were used to represent the present-day mean fire state.

In addition to burned area, we calculated the number of fires and mean fire size in each 1° grid cell in the Alaskan and Canadian parts of the circumpolar boreal region. In Alaska, we used historical fire information from the Alaska Interagency Coordination Center (<https://fire.ak.blm.gov>), which provides data on the annual total burned area and number of fires. Fire number and size information in Canada was from the Canadian National Fire Database in the Canadian Wildland Fire Information System (<http://cwfis.cfs.nrcan.gc.ca/>). Because data from earlier years may suffer from lower quality and incomplete coverage, we used both datasets for the years 2000–2016 to represent the present-day ecosystem state. Fires were binned in 1° × 1° grid cells on the basis of their centroid locations.

Future projection of burned area and fire emissions. Since lightning is the major source of ignition in the boreal region, we expect that the future increase of lightning flash rate will lead to more fires and larger areas burned annually. On the basis of different assumptions of fire response to lightning ignition, we explored two approaches to estimate burn area distribution in the circumpolar boreal region in the future warming climate. In the first approach (static vegetation), we assumed that the burned area associated with each flash varies as a function of the distance to the northern treeline, and that the burned-area-to-flash-rate ratio remains unchanged in each location under global warming. On the basis of present-day observations, we calculated the ratio of burned area to lightning flash rate (r) for each grid cell and derived a parameterization of r as a function of distance north of the treeline (d): $r = f(d)$. We then used the estimated future lightning flash rate (FR_n) to project the future distribution of burned area (BA_n): $BA_n = FR_n \times f(d)$.

In the second approach (dynamic vegetation), we assumed that the northern treeline will have a northward displacement in future climate, and therefore the sensitivity of burned area to lightning will also shift north as a consequence of vegetation and climate feedback. Figure 3a shows that the future flash rates at the present northern treeline in 2100 will be comparable to contemporary levels occurring 480 km to the south. Here we assume that the profile of parameterized r will shift north by 480 km along the distance north of the treeline at the end of this century: $r = f(d - 480 \text{ km})$ (Extended Data Fig. 8). The revised r profile was used to provide future burned area estimation in the dynamic vegetation approach.

The amount of soil carbon loss per unit area of tundra burning is substantially influenced by the fire severity and the depth of the surface organic layer. Mack et al.²⁰ studied a large tundra wildfire near the Anaktuvuk River of Alaska during the summer of 2007 and reported that tundra ecosystems currently lose about 2.0 kg C per m² of burned area. While a complete dataset in the whole Arctic tundra biome is not presently available, here we applied the scaler from the Anaktuvuk data to the burned area estimates described above, and we derived a first-order estimation of changes in total carbon emissions.

Other data. Several surface maps from high-northern-latitude regions were used to further study the response of vegetation dynamics and the carbon cycle to the projected changes in lightning. The location of the northern treeline was defined using the Circumpolar Arctic Coastline and Treeline Boundary dataset from the Circumpolar Arctic Vegetation Map (<http://www.arcticatlas.org/maps/themes/cp/cpcoast>)⁸⁹.

The Northern Circumpolar Soil Carbon Database version 2 (<https://bolin.su.se/data/nscsd/>) provided gridded information on the fractional coverage of different soil types and storage of soil organic carbon³. Here we defined the permafrost soil carbon as the total storage of carbon between 0 and 100 cm deep from this dataset.

Data availability

The LIS/OTD lightning data products are from the NASA Global Hydrology Resource Center website (https://lightning.nsstc.nasa.gov/data/data_lis-otd-climatology.html), the CMIP5 meteorological data are from the Earth System Grid Federation (<https://esgf-node.llnl.gov/search/cmip5/>) and the burned-area data are from the Global Fire Emissions Database (<http://www.globalfiredata.org/>), the Alaska Interagency Coordination Center (<https://fire.ak.blm.gov>) and the Canadian Wildland Fire Information System (<http://cwfis.cfs.nrcan.gc.ca/>). Other data supporting the findings of this study are available within the paper and its supplementary information files. Source data are provided with this paper.

Code availability

The code used for the lightning and burned area analysis is available from the corresponding author upon request.

References

- Friedl, M. A. et al. MODIS Collection 5 global land cover: algorithm refinements and characterization of new datasets. *Remote Sens. Environ.* **114**, 168–182 (2010).
- Mach, D. M. et al. Performance assessment of the Optical Transient Detector and Lightning Imaging Sensor. *J. Geophys. Res.* **112**, D09210 (2007).
- Mackerras, D., Darveniza, M., Orville, R. E., Williams, E. R. & Goodman, S. J. Global lightning: total, cloud and ground flash estimates. *J. Geophys. Res.* **103**, 19791–19809 (1998).
- Farukh, M. A. & Hayasaka, H. Active forest fire occurrences in severe lightning years in Alaska. *J. Nat. Disaster Sci.* **33**, 71–84 (2012).
- Hersbach, H. et al. The ERA5 global reanalysis. *Q. J. R. Meteorol. Soc.* **146**, 1999–2049 (2020).
- Taylor, K. E., Stouffer, R. J. & Meehl, G. A. An overview of CMIP5 and the experiment design. *Bull. Am. Meteorol. Soc.* **93**, 485–498 (2012).
- Seeley, J. T. & Roms, D. M. The effect of global warming on severe thunderstorms in the United States. *J. Clim.* **28**, 2443–2458 (2015).
- van Vuuren, D. P. et al. The representative concentration pathways: an overview. *Climatic Change* **109**, 5–31 (2011).
- Chronis, T. G. et al. Global lightning activity from the ENSO perspective. *Geophys. Res. Lett.* **35**, L19804 (2008).
- Satori, G., Williams, E. & Lempferger, I. Variability of global lightning activity on the ENSO time scale. *Atmos. Res.* **91**, 500–507 (2009).
- Randerson, J. T., Chen, Y., van der Werf, G. R., Rogers, B. M. & Morton, D. C. Global burned area and biomass burning emissions from small fires. *J. Geophys. Res. Biogeosci.* **117**, G04012 (2012).
- van der Werf, G. R. et al. Global fire emissions estimates during 1997–2016. *Earth Syst. Sci. Data* **9**, 697–720 (2017).
- Walker, D. A. et al. The circumpolar Arctic vegetation map. *J. Veg. Sci.* **16**, 267–282 (2005).

Acknowledgements

This work was supported by the US Department of Energy (DOE) Office of Science Biological and Environmental Research RUBISCO Science Focus Area (with funding to J.T.R., Z.A.M. and W.J.R.), the NGE- Arctic project (with funding to Z.A.M. and W.J.R.) and NASA's Interdisciplinary Science (IDS) and Carbon Monitoring System (CMS) programmes (with grants to J.T.R. and Y.C.). D.M.R. was supported by the US DOE Atmospheric System Research (ASR), an Office of Science, Office of Biological and Environmental Research programme. Lawrence Berkeley National Laboratory is operated for the DOE by the University of California under contract no. DE-AC02-05CH11231. We thank the World Climate Research Programme Working Group on Coupled Modeling, responsible for CMIP, and we thank the climate modelling groups for generating their model outputs and making them available.

Author contributions

Y.C. and J.T.R. designed the study. Y.C. led the research and performed the analyses described in the main text and supporting information. D.M.R. and J.T.S. derived the lightning index (CAPE × Precip) from meteorological variables archived from historical and RCP8.5 ESM simulations contributed to CMIP5. S.V. contributed to the development of the lightning model and to the conceptual model of a lightning-initiated dynamic vegetation feedback. W.J.R. and Z.A.M. contributed to the conceptual model of the dynamic vegetation feedback and to the discussion of the implications of a changing lightning regime for terrestrial ecosystems. All authors contributed to the writing and review of the manuscript.

Competing interests

The authors declare no competing interests.

Additional information

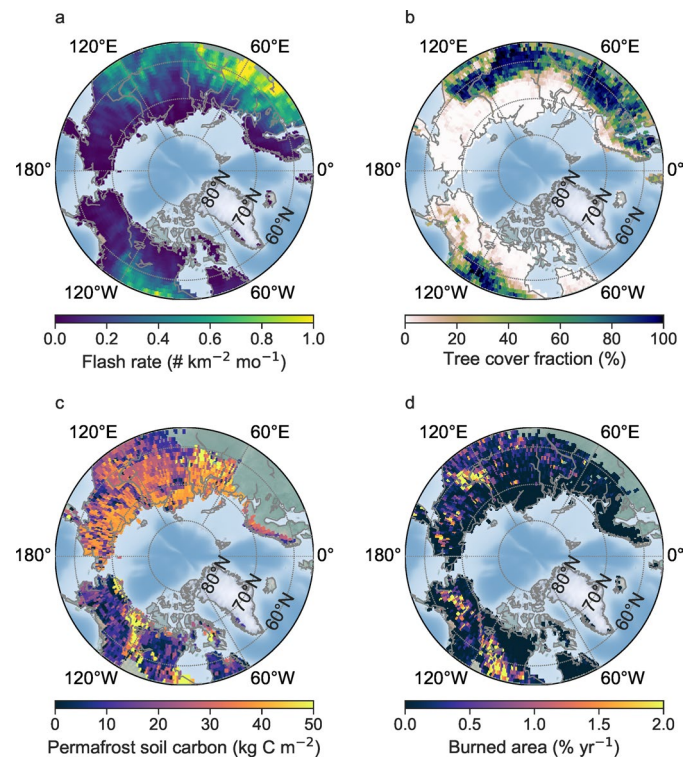
Extended data is available for this paper at <https://doi.org/10.1038/s41558-021-01011-y>.

Supplementary information The online version contains supplementary material available at <https://doi.org/10.1038/s41558-021-01011-y>.

Correspondence and requests for materials should be addressed to Y.C.

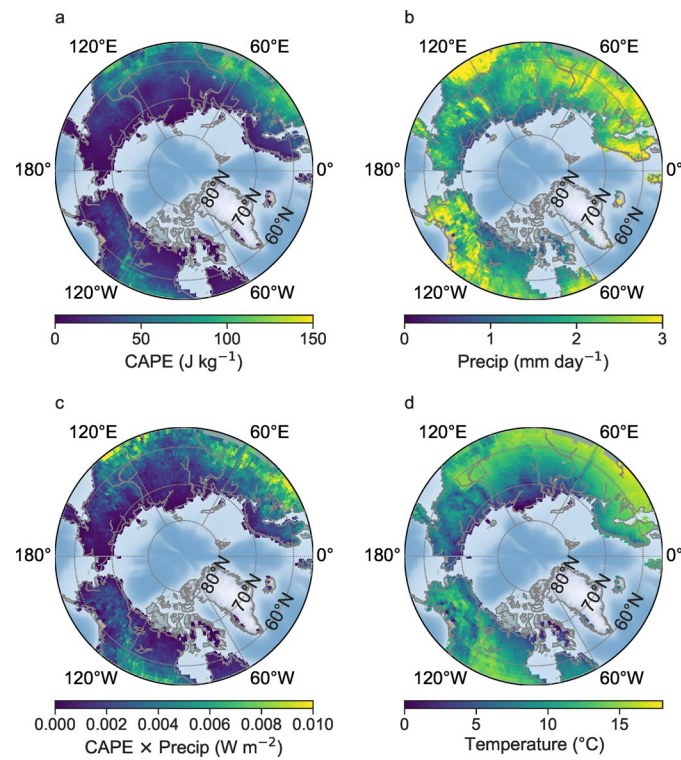
Peer review information *Nature Climate Change* thanks the anonymous reviewers for their contribution to the peer review of this work.

Reprints and permissions information is available at www.nature.com/reprints.

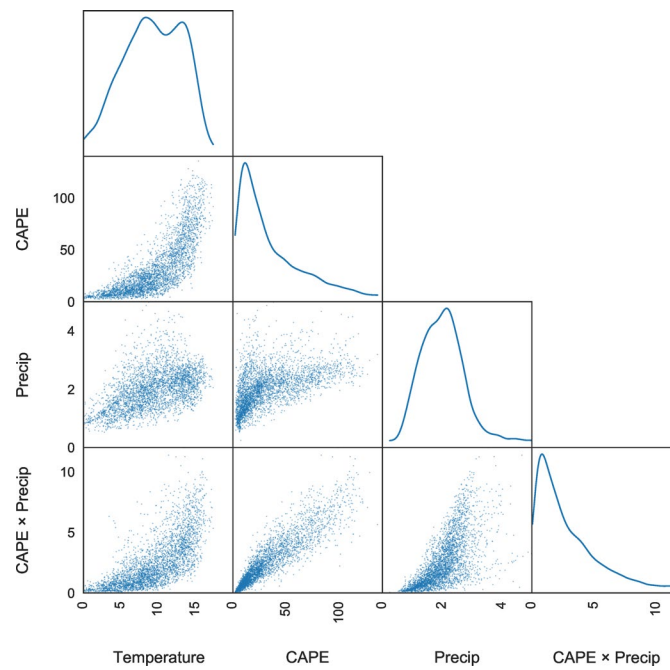


Extended Data Fig. 1 | Circumpolar observations of present-day lightning flash rate, tree cover fraction, permafrost soil carbon, and burned area.

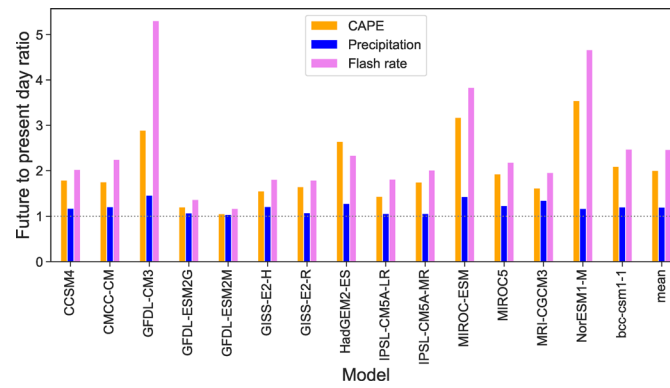
a, lightning flash rate (# km⁻² mo⁻¹, from OTD, averaged over May-August of 1996-1999); **b**, tree cover fraction (%), based on MODIS observations in 2012); **c**, permafrost soil carbon at depth of 0-100 cm (kg C m⁻², from NCSCDv2); and **d**, burned area (% yr⁻¹, from GFED4s, averaged over 1996-2016) in high northern latitude regions (north of 55°N).



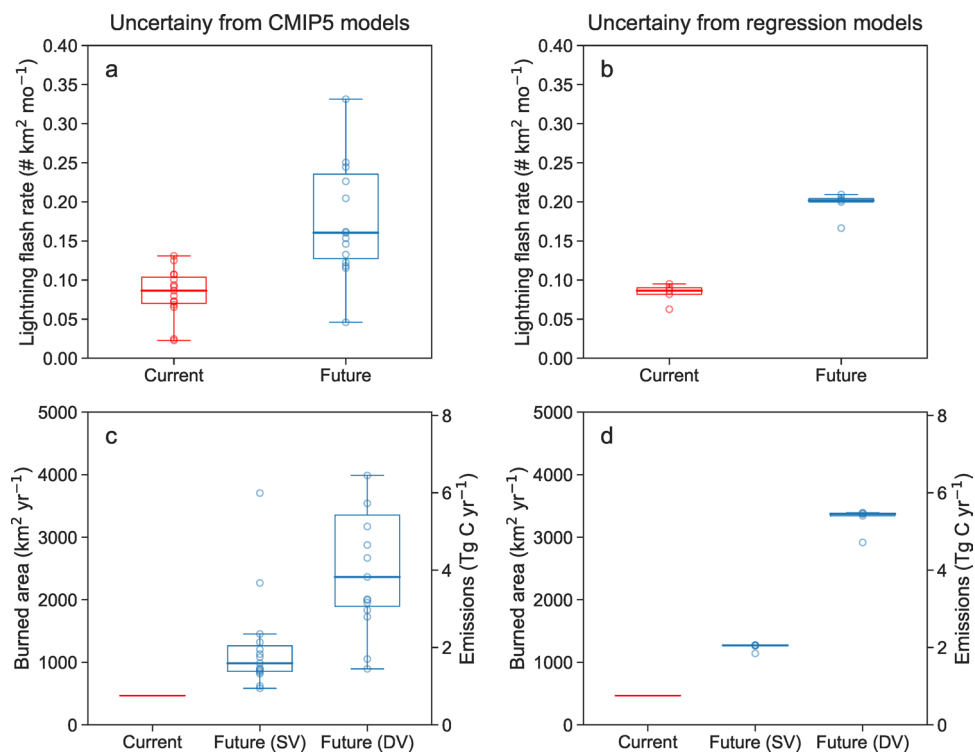
Extended Data Fig. 2 | Circumpolar observations of meteorological parameters. Maps of **a**, CAPE (J kg^{-1}); **b**, precipitation (Precip, mm day^{-1}); **c**, CAPE \times Precip (W m^{-2}); and **d**, surface air temperature ($^{\circ}\text{C}$) in high northern latitude regions of 55°N , representing the mean of summers (May-August) during 1996-1999. All meteorological parameters are from the ERA5 global reanalysis dataset.



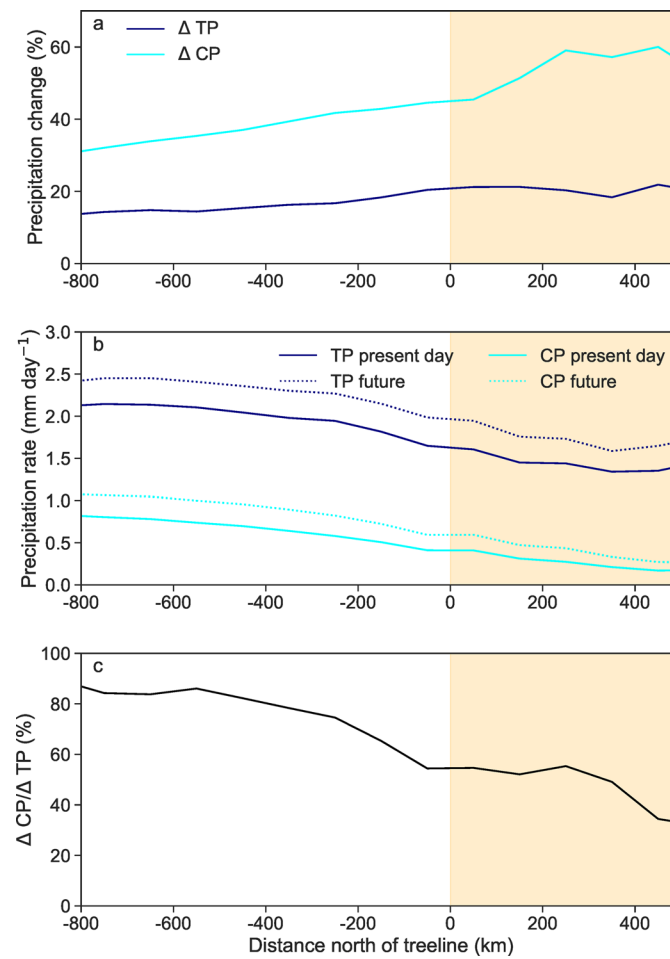
Extended Data Fig. 3 | Scatter plot relationships and probability distribution functions for meteorological variables known to be important for lightning flash rate prediction. The surface air temperature (T) is in $^{\circ}\text{C}$, CAPE is in J kg^{-1} , precipitation (Precip) is in mm day^{-1} , and $\text{CAPE} \times \text{Precip}$ is in 10^{-3}W m^{-2} . Each point represents a different spatial location (at a $1^{\circ} \times 1^{\circ}$ resolution) north of 55°N . Diagonal panels show the spatial probability distribution for each variable, created by taking the mean at each point during summers (May–August) of 1996–1999. All meteorological parameters are from the ERA5 global reanalysis dataset.



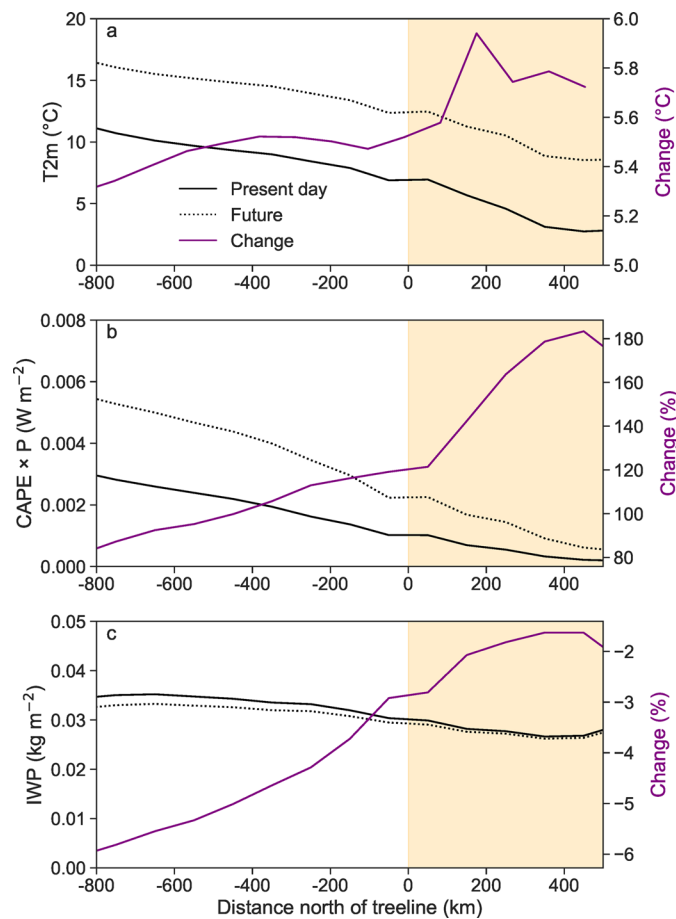
Extended Data Fig. 4 | Future (2081-2100) to the present day (1986-2005) ratios of CAPE, precipitation, and lightning flash rate in Arctic tundra for different CMIP5 models. The mean flash rate values calculated from 5 regression formula (see Supplementary Table 2) are shown for each CMIP5 model.



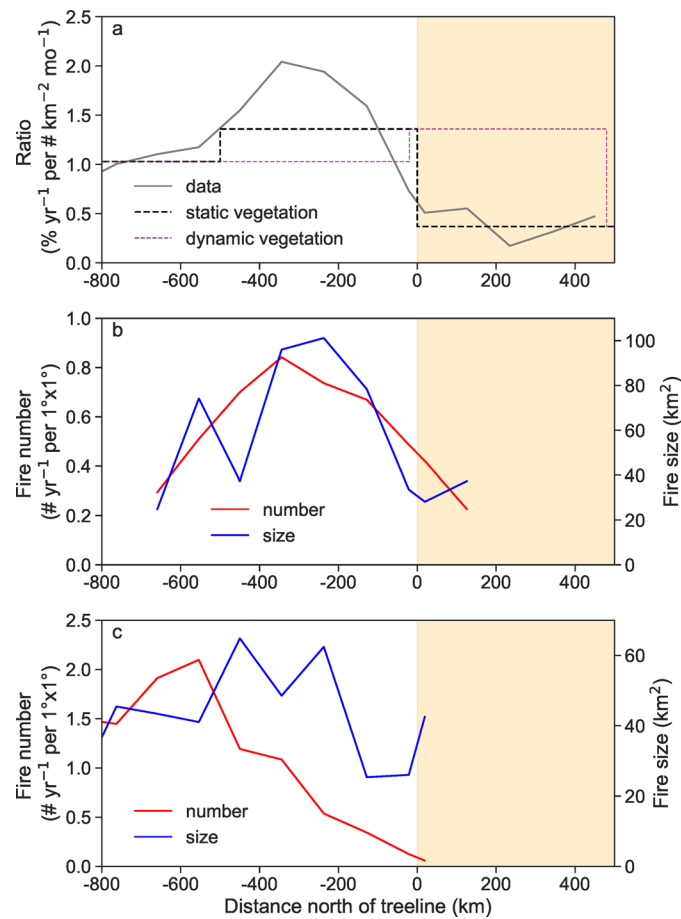
Extended Data Fig. 5 | Sources of uncertainty for estimated lightning flash rates, burned area and carbon emissions. The flash rates were averaged over the Arctic tundra region. The burned area and carbon emissions were averaged over the Arctic tundra region within 500 km of northern treeline as indicated in Fig. 3. Left panels show uncertainties due to the use of CAPE × Precipitation from the use of multiple CMIP5 model simulations. Right panels show uncertainties related to the use of statistical models relating flash rate and CAPE × Precipitation. SV and DV represents future burned area estimations using the ‘static vegetation’ and ‘dynamic vegetation’ approaches (see Methods and Supplementary Table 3 for detail). Note the burned area and carbon emissions have same data distribution but with different units and scales.



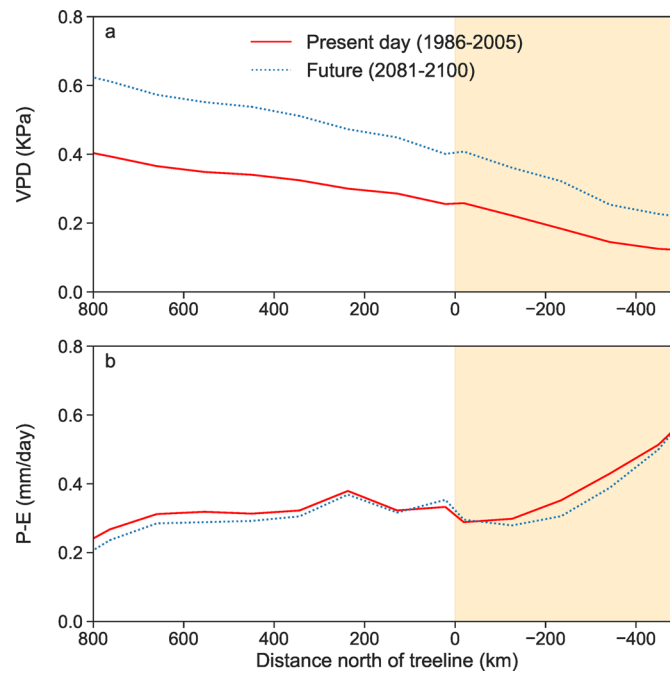
Extended Data Fig. 6 | Present day and future estimates of total precipitation (TP) and convective precipitation (CP) as a function of distance from northern treeline. a, TP and CP percent changes from present day to the future. **b,** TP and CP values for the present day and future. **c,** The fraction of TP change that is due to CP change. The orange shade indicates the Arctic tundra region 0-500 km north of treeline. All data are based on the ensemble means of 15 CMIP5 model simulations over 1986-2005 and 2081-2100.



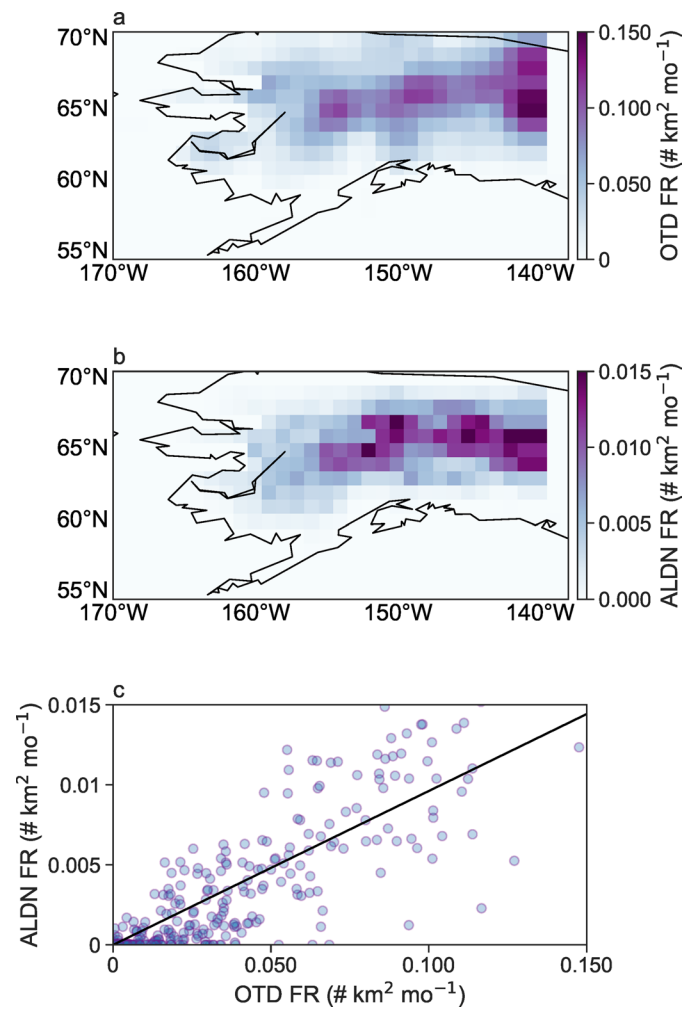
Extended Data Fig. 7 | Distributions of surface temperature, CAPE × Precip, and the ice water path as a function of distance north of treeline. a, surface temperature (T2m), **b,** the product of CAPE and precipitation (CAPE × Precip) and **c,** the ice water path (IWP) were calculated during summers for a contemporary period (1986-2005) and a future period (2081-2100). The percent changes are relative to the mean values during the contemporary period. The orange shade indicates the Arctic tundra region 0-500 km north of treeline. All data are based on the ensemble means of 15 CMIP5 model simulations over 1986-2005 and 2081-2100.



Extended Data Fig. 8 | Contemporary lightning and wildfire properties as a function of distance from northern treeline. **a**, The ratio of burned area (BA) to lightning flash rate (FR). Black dashed line represents parameterized step function ('static vegetation'). Purple dashed line shows the shifted step function used for future burned area estimation ('dynamic vegetation'). **b**, Fire number and mean fire size in Alaska, as reported by Alaska Interagency Coordination Center for the period of 2000 to 2016. **c**, Fire number and mean fire size in Canada, as reported by Canadian Wildland Fire Information System during the same period. The orange shade denotes the Arctic tundra region that may be vulnerable to future changes in lightning, burned area, and vegetation dynamics (0-500 km north of treeline).



Extended Data Fig. 9 | Vapor pressure deficit (VPD) and the difference between precipitation and evapotranspiration (P-E) as a function of distance from northern treeline. The VPD and P-E values are derived from the ensemble mean meteorology of 15 CMIP5 model simulations over 1986-2005 and 2081-2100.



Extended Data Fig. 10 | Comparison of lightning flash rates measured by satellite and a surface network in Alaska during summers of 1996-1999.

a, Flash rate ($\# \text{ deg}^{-1} \text{ mo}^{-1}$) recorded by the Optical Transient Detector (OTD), **b**, Flash rate ($\# \text{ deg}^{-1} \text{ mo}^{-1}$) from the Alaskan Lightning Detection Network (ALDN), **c**, Spatial correlation between the flash rates from OTD and ALDN. Each dot represents the mean summer value in a $1^\circ \times 1^\circ$ grid cell in Alaska.